journals.elsevier.com/applied-surface-science

ELSEVIER

About Elsevier | Products & Solutions | Services | Shop & Discover | Search

Home > Journals > Applied Surface Science

ISSN: 0169-4332

Applied Surface Science

A Journal Devoted to Applied Physics and Chemistry of Surfaces and Interfaces

> Elsevier Physics homepage

Publishing options: OA Open Access ↗ S Subscription ↗

↗ Guide for authors Track your paper ⌄ ↗ Order journal

Editor-in-Chief > Editorial board

H. Rudolph, PhD

Submit your paper

The Impact Factor of this journal is 6.707, ranking it 1 out of 21 in *Materials Science, Coatings & Films*

With this journal indexed in 11 international databases, your published article can be read and cited by researchers worldwide

View articles

sciencedirect.com/journal/applied-surface-science/vol/466/suppl/C

Frans Habraken Best Paper Award 2022
Call for nominations now open
ELSEVIER
Applied Surface Science
Visit Journal homepage for more details

ScienceDirect

Journals & Books | Register | Sign in

Applied Surface Science

Supports *open access*

10.7 CiteScore | 6.707 Impact Factor

Articles & Issues ⌄ | About ⌄ | Publish ⌄ | Order journal ↗ | Search in this journal | Submit your article ↗ | Guide for authors ↗

Volume 466

Pages 1-1006 (1 February 2019)

< Previous vol/issue | Next vol/issue >

APPLIED SURFACE SCIENCE

A journal devoted to applied physics and chemistry of surfaces and interfaces

Founding Editor: R.L. Park

Editors

Henrik Rudolph 'Editor-in-Chief'
Faculty of Military Sciences (FMS)
Netherlands Defence Academy
PO Box 90002, 4800 PA Breda
The Netherlands
E-mail: h.rudolph@apsusc.com

Stephan Barcikowksi
Universität Duisburg-Essen, Essen, Germany
E-mail: stephan.barcikowski@nano-manufacturing.de

Maria Dinescu
National Institute for Lasers
Plasma and Radiation Physics
Str. Atomistilor, Nr. 409
PO Box MG-36, 077125
Magurele, Bucharest, Romania
E-mail: dinescum@nipne.ro

Qiang Fu
State Key Laboratory of Catalysis (SKLC)
Dalian Institute of Chemical Physics (DICP)
Chinese Academy of Sciences (CAS)
457 Zhongshan Road 116023 Dalian, P.R. China
E-mail: qfu@dicp.ac.cn

Guido Grundmeier
Technische und Makromolekulare Chemie,
Universität Paderborn Warburger
Str. 100 3309 Paderborn
E-mail: guido.grundmeier@uni-paderborn.de

Weixin Huang
Department of Chemical Physics
University of Science and Technology of China
Hefei 230026 China
E-mail: huangwx@ustc.edu.cn

Alfredo Juan
Departamento de Fisica & IFISUR (UNS-CONICET),
Universidad Nacional del Sur,
Av. Alem 1253, 8000 Bahia Blanca, Argentina
E-mail: cajuan@uns.edu.ar

Peter Kingshott
Swinburne University of Technology
Fac. of Engineering & Industrial Sciences
P.O. Box 218, 543-454 Burwood Road Hawthorn,
VIC 3122, Australia
E-mail: pkingshott@swin.edu.au

Tadahiro Komeda
Institute of Multidisciplinary Research
for Advanced Materials (IMRAM)
Tohoku University
2-1-1, Katahira, Aoba,
Sendai 980-0877, Japan
E-mail: komeda@tagen.tohoku.ac.jp

Matthew R. Linford
Department of Chemistry and Biochemistry
C100 BNSN (Benson Science Building)
Brigham Young University, Provo, UT 84602, USA
E-mail: mrlinford@chem.byu.edu

Chris F. McConville
College of Science, Engineering & Health RMIT
University Melbourne, VIC 3001, Australia
E-mail: chris.mcconville@rmit.edu.au

Fátima Montemor
Instituto Superior Tecnico ICEMS-DEQ Avenida Rovisco Pais
1049-001 Lisboa, Portugal
E-mail: mfmontemor@ist.utl.pt

Robert L. Opila
University of Delaware Materials Science and
Engineering Dupont Hall 210 Newark DE 19716, USA
E-mail: opila@uDel.edu

Jacques Perriere
Universite P&M Curie (UPMC) Institut des Nano Sciences de
Paris 4 Place Jussieu, Paris, 75252
Paris Cedex 05, France
E-mail: jacques.perriere@insp.jussieu.fr

Nini Pryds
Technical University of Denmark Electro-Functional
Materials Department of Energy Conversion and
Storage Roskilde, Denmark
E-mail: nipr@dtu.dk

Mario Rocca
Dept. of Physics Università degli Studi di Genova via
Dodecaneso 33, 16146, Genova, Italy
E-mail: rocca@fisica.unige.it

Peter Schaaf
Institute of Materials Engineering and
Institute of Micro- and Nanotechnologies
Technische Universität Ilmenau
Gustav-Kirchhoff-Str. 5, 98693 Ilmenau, Germany
E-mail: applsurfscience@technocon-schaaf.de

Yang Shen
School of Materials Science and Engineering,
Tsinghua University, Beijing, China
E-mail: shyang_mse@mail.tsinghua.edu.cn

Franklin (Feng) Tao
Department of Chemical and Petroleum Engineering
Department of Chemistry University of Kansas
Lawrence KS 66047, USA Tel: (785) 864-7273
Email: franklin.feng.tao@ku.edu

Andrew Teplyakov
Department of Chemistry and Biochemistry
University of Delaware 112 Lammot du Pont Laboratory
Newark, DE 19716, USA
E-mail: andrewt@udel.edu

Jeff Terry
Department of Physics, Illinois Institute of Technology,
3101 S. Dearborn St., Chicago, Illinois, USA
E-mail: terryj@iit.edu

Herbert Urbassek
Physics Department and Research Center OPTIMAS
University Kaiserslautern, Kaiserslautern, Germany
E-mail: urbassek@rhrk.uni-kl.de

Robert M. Wallace
Department of Materials Science and Engineering
University of Texas at Dallas Richardson, Texas 75083, USA
E-mail: rmwallace@utdallas.edu

James E. Whitten
Department of Chemistry University of Massachusetts
Lowell One University Avenue Lowell, MA 01854, USA
E-mail: James_Whitten@uml.edu

Jiaguo Yu
State Key Laboratory of Advanced Technology for
Materials Synthesis and Processing
Wuhan University of Technology
Luoshi Road 122#, Wuhan, 430070, P.R. China
E-mail: jiaguoyu@yahoo.com; yujiaguo93@163.com

Advisory Editorial Board

Argentina
Alfredo Juan, Bahia Blanca

Belgium
Rino Morent, Ghent

Canada
Gregory Lopinski, Ontario Federico Rosei,
Lionel Boulet

China
Dongdong Gu, Nanjing Jianshe Lian,
Changchun Weitao Zheng, Changchun

Denmark
Nini Pryds, Roskilde

France
Jacques (J.) Perrière, Paris

Germany
Stephan Barcikowski,
Essen Siegfried Hofmann,
Stuttgart Patrik Schmuki, Erlangen

Greece
Costas Fotakis, Heraklion

India
Bhupendra Dev, Kolkata

Italy
Antonio Miotello, Povo (Trento)

Japan
Katsuhiro Akimoto, Ibaraki
Akira Nakajima, Tokyo

Portugal
Elvira Fortunato, Lisbon

New Zeeland
Hendrik Swart, Bloemfontein

Singapore
Chang Quing Sun, Singapore
Xiao Wei Sun, Singapore

Slovak Republic
Emil Pincik, Bratislava

Switzerland
Yves Leterrier, Lausanne

The Netherlands
Harold Zandvliet, Enschede
Han Zuilhof, Wageningen

Turkey
Sefik Suzer, Ankara

UK
Hans Niemantsverdriet, Cardiff Alex Shard,
Teddington

USA
David Aspnes, Raleigh, NC
Teresa Bandosz, New York, NY
Amit Bandyopadhyay, WA
Yongli Gao, New York, NY
Jeffrey Greeley, West Lafayette
Steve Pearton, Gainesville, IN
Leonid Zhigilei, Charlottesville, VA

ScienceDirect

Applied Surface Science

Supports *open access*

12.1
CiteScore

6.707
Impact Factor

Submit your article

Guide for authors

Menu

Search in this journal

Volume 466

Pages 1-1006 (1 February 2019)

Previous vol/issue

Next vol/issue

Receive an update when the latest issues in this journal are published

Sign in to set up alerts

Full text access

Editorial Board

Page ii

Download PDF

Full Length Article

Research article ○ Abstract only

FEEDBACK

FEEDBACK

FEEDBACK

Purchase PDF Article preview

Research article ○ Abstract only

Interface engineering of Co_3O_4 loaded $CaFe_2O_4/Fe_2O_3$ heterojunction for photoelectrochemical water oxidation

Jiajia Cai, Song Li, Gaowu Qin

Pages 92-98

Purchase PDF Article preview

Research article ○ Abstract only

New insight into alkali resistance and low temperature activation on vanadia-titania catalysts for selective catalytic reduction of NO

Shuo Zhang, Shaojun Liu, Wenshuo Hu, Xinbo Zhu, ... Xiang Gao

Pages 99-109

Purchase PDF Article preview

Research article ○ Abstract only

Polyoxometalate-coupled graphene nanohybrid via gemini surfactants and its electrocatalytic property for nitrite

Shu Chen, Yuanfang Xiang, M. Katherine Banks, Weijian Xu, ... Ruoxi Wu

Pages 110-118

Purchase PDF Article preview

Research article ○ Abstract only

Quantum confinement luminescence of trigonal cesium lead bromide quantum dots

Yumeng Zhang, Yuanyuan Li, Yuzhen Liu, Hongxia Li, Jiyang Fan

Pages 119-125

Purchase PDF Article preview

Research article ○ Abstract only

Robust $Mg(OH)_2$/epoxy resin superhydrophobic coating applied to composite insulators

Wenyu Peng, Xuelian Gou, Hongling Qin, Meiyun Zhao, ... Zhiguang Guo

Pages 126-132

Purchase PDF Article preview

FEEDBACK

Research article ○ Abstract only

A Z-scheme mechanism of N-ZnO/g-C_3N_4 for enhanced H_2 evolution and photocatalytic degradation

Yujie Liu, Haixia Liu, Huamin Zhou, Tianduo Li, Lunan Zhang

Pages 133-140

Purchase PDF Article preview

Research article ○ Abstract only

6H-SiC blistering efficiency as a function of the hydrogen implantation fluence

N. Daghbouj, B.S. Li, M. Karlik, A. Declemy

Pages 141-150

Purchase PDF Article preview

Research article ○ Abstract only

Investigation of complex residual stress states in the near-surface region: Evaluation of the complete stress tensor by X-ray diffraction pattern decomposition

Peter Schoderböck

Pages 151-164

Purchase PDF Article preview

Research article ○ Abstract only

Corrosion behavior of a β CuAlBe shape memory alloy containing stress induced martensite

S. Montecinos, P. Klímek, M. Sláma, S. Suarez, S. Simison

Pages 165-170

Purchase PDF Article preview

Research article ○ Abstract only

Preparation and characterization of a durable superhydrophobic hyperbranched poly(dimethylolbutanoic acid-glycidyl ester of versatic acid)/nano-SiO_2 coating

Han Cui, Mingguang Hu, Zhen Yu, Jijun Xiao

Pages 171-178

Purchase PDF Article preview

Research article ○ Abstract only

FEEDBACK

FEEDBACK

FEEDBACK

FEEDBACK

Purchase PDF Article preview

Research article ○ Abstract only

Use of Mn doping to suppress defect sites in Ag_3PO_4: Applications in photocatalysis

Mohammad Afif, Uyi Sulaeman, Anung Riapanitra, Roy Andreas, Shu Yin

Pages 352-357

Purchase PDF Article preview

Research article ○ Abstract only

Studies on the graded band-gap copper indium di-selenide thin film solar cells prepared by electrochemical route

Ashwini B. Rohom, Priyanka U. Londhe, Jeong In Han, Nandu B. Chaure

Pages 358-366

Purchase PDF Article preview

Research article *Open access*

MWCNTs produced by electrolysis of molten carbonate: Characteristics of the cathodic products grown on galvanized steel and nickel chrome electrodes

S. Arcaro, F.A. Berutti, A.K. Alves, C.P. Bergmann

Pages 367-374

Download PDF Article preview

Research article ○ Abstract only

Dissolution of thin TaV_2 during annealing of $Ta/TaV_2/V$ tri-layer below the order-disorder temperature

A. Csík, S.S. Shenouda, Z. Erdélyi, D.L. Beke

Pages 381-384

Purchase PDF Article preview

Research article ○ Abstract only

Graphene-templated synthesis of palladium nanoplates as novel electrocatalyst for direct methanol fuel cell

Hujiang Yang, Liang Geng, Yuting Zhang, Gang Chang, ... Yunbin He

Pages 385-392

Purchase PDF Article preview

FEEDBACK

Research article ○ Abstract only

Improving the intrinsic properties of rGO sheets by S-doping and the effects of rGO improvements on the photocatalytic performance of Cu_3Se_2/rGO nanocomposites

Mohammad Amin Baghchesara, H.R. Azimi, A. Ghorban Shiravizadeh, Mohd Asri Mat Teridi, Ramin Yousefi

Pages 401-410

Purchase PDF Article preview

Research article ○ Abstract only

Improvement of activity, selectivity and H_2O&SO_2-tolerance of micro-mesoporous $CrMn_2O_4$ spinel catalyst for low-temperature NH_3-SCR of NOx

Fengyu Gao, Xiaolong Tang, Honghong Yi, Shunzheng Zhao, ... Tian Gu

Pages 411-424

Purchase PDF Article preview

Research article ○ Abstract only

Competitive adsorption of arsenic and fluoride on {2 0 1} TiO_2

Zhen Zhou, Yaqin Yu, Zhaoxia Ding, Meimei Zuo, Chuanyong Jing

Pages 425-432

Purchase PDF Article preview

Research article ○ Abstract only

Electrodeposition of Ni-Mo/Al_2O_3 nano-composite coatings at various deposition current densities

Morteza Alizadeh, Abbas Cheshmpish

Pages 433-440

Purchase PDF Article preview

Research article ○ Abstract only

Slip trace-induced terrace erosion

Benjamin Douat, Jérôme Colin, Roberto Bergamaschini, Francesco Montalenti, ... Christophe Coupeau

Pages 454-458

Purchase PDF Article preview

Research article ○ Abstract only

FEEDBACK

FEEDBACK

The spatial inhomogeneity and X-ray absorption spectroscopy of superconducting nanocrystalline boron doped diamond films

Dinesh Kumar, G. Mangamma, Martando Rath, M.S. Ramachandra Rao

Pages 498-502

Purchase PDF Article preview

Research article ○ Abstract only

The verification of icephobic performance on biomimetic superhydrophobic surfaces and the effect of wettability and surface energy

Wenjuan Cui, Yu Jiang, Kati Mielonen, Tapani A. Pakkanen

Pages 503-514

Purchase PDF Article preview

Research article ○ Abstract only

Carbon quantum dots sensitized $ZnSn(OH)_6$ for visible light-driven photocatalytic water purification

Yuanyuan Zhang, Lili Wang, Manli Yang, Jie Wang, Jinsheng Shi

Pages 515-524

Purchase PDF Article preview

Research article ○ Abstract only

In-situ preparation of NH_2-MIL-125(Ti)/BiOCl composite with accelerating charge carriers for boosting visible light photocatalytic activity

Qingsong Hu, Jun Di, Bin Wang, Mengxia Ji, ... Yaping Zhao

Pages 525-534

Purchase PDF Article preview

Research article ○ Abstract only

Synthesis and visible-light photocatalytic CO_2/H_2O reduction to methyl formate of TiO_2 nanoparticles coated by aminated cellulose

Halidan Maimaiti, Abuduheiremu Awati, Gunisakezi Yisilamu, Dedong Zhang, Shixin Wang

Pages 535-544

Purchase PDF Article preview

Research article ○ Abstract only

FEEDBACK

FEEDBACK

Interaction between polysaccharide monomer and $SiO_2/Al_2O_3/CaCO_3$ surfaces: A DFT theoretical study

Hui Zhao, Na Qi, Ying Li

Pages 607-614

Purchase PDF Article preview

Research article ○ Abstract only

Synthesis and modification of Cu-C_{70} nanocomposite for plasmonic applications

Rahul Singhal, Satakshi Gupta, Ritu Vishnoi, Ganesh D. Sharma

Pages 615-627

Purchase PDF Article preview

Research article ○ Abstract only

Gradient multifunctional biopolymer thin film assemblies synthesized by combinatorial MAPLE

Natalia Mihailescu, Merve Erginer Haskoylu, Carmen Ristoscu, Müge Sennaroglu Bostan, ... Ion N. Mihailescu

Pages 628-636

Purchase PDF Article preview

Research article ○ Abstract only

Core-shell dual-MOF heterostructures derived magnetic $CoFe_2O_4/CuO$ (sub)microcages with superior catalytic performance

Yan-Feng Huang, Xiao-Yi Sun, Shu-Hui Huo, Ying Li, Chongli Zhong

Pages 637-646

Purchase PDF Article preview

Research article ○ Abstract only

Constructing multiple interfaces in polydimethylsiloxane/multi-walled carbon nanotubes nanocomposites by the incorporation of cotton fibers for high-performance electromagnetic interference shielding and mechanical enhancement

Jie Li, Yan-Jun Tan, Yi-Fu Chen, Hong Wu, ... Ming Wang

Pages 657-665

Purchase PDF Article preview

Research article ○ Abstract only

FEEDBACK

A g-C_3N_4@ppy-rGO 3D structure hydrogel for efficient photocatalysis
Yinghua Liang, Xing Wang, Weijia An, Yao Li, ... Wenquan Cui
Pages 666-672

Purchase PDF Article preview

Research article ○ Abstract only

Surface doping of the $LaMg_3$ alloy with nano-cobalt particles for promoting the hydrogenation properties through magnetron sputtering
Huaiwei Zhang, Li Fu, Weidong Xuan, Zhenguo Ji
Pages 673-678

Purchase PDF Article preview

Research article ○ Abstract only

Bio-surfactant assisted solvothermal synthesis of Magnetic retrievable Fe_3O_4@rGO nanocomposite for photocatalytic reduction of 2-nitrophenol and degradation of TCH under visible light illumination
S. Mansingh, D.K. Padhi, Kulamani Parida
Pages 679-690

Purchase PDF Article preview

Research article ○ Abstract only

Effect of aminated nanocrystal cellulose on proton conductivity and dimensional stability of proton exchange membranes
Qi Zhao, Yingcong Wei, Chuangjiang Ni, Lele Wang, ... Yunfeng Lu
Pages 691-702

Purchase PDF Article preview

Research article ○ Abstract only

Tuning the morphology of Cr_2O_3:CuO (50:50) thin films by RF magnetron sputtering for room temperature sensing application
S. Ponmudi, R. Sivakumar, C. Sanjeeviraja, C. Gopalakrishnan, K. Jeyadheepan
Pages 703-714

Purchase PDF Article preview

Research article ○ Abstract only

FEEDBACK

FEEDBACK

FEEDBACK

Modified strain and elastic energy behavior of Ge islands formed on high-miscut Si(0 0 1) substrates

L.A.B. Marçal, M.-I. Richard, L. Persichetti, V. Favre-Nicolin, ... A. Malachias

Pages 801-807

Download PDF Article preview

Research article ○ Abstract only

Long term superhydrophobic and hybrid superhydrophobic/superhydrophilic surfaces produced by laser surface micro/nano surface structuring

Fatema H. Rajab, Zhu Liu, Lin Li

Pages 808-821

Purchase PDF Article preview

Research article ○ Abstract only

Chemically synthesized nanoflakes-like $NiCo_2S_4$ electrodes for high-performance supercapacitor application

S.K. Shinde, M.B. Jalak, G.S. Ghodake, N.C. Maile, ... D.-Y. Kim

Pages 822-829

Purchase PDF Article preview

Research article ○ Abstract only

Three dimensional flower like cobalt sulfide (CoS)/functionalized MWCNT composite catalyst for efficient oxygen evolution reactions

K. Prabakaran, Moorthi Lokanathan, Bhalchandra Kakade

Pages 830-836

Purchase PDF Article preview

Research article ○ Abstract only

Amorphous Fe_2O_3 nanoparticles embedded into hypercrosslinked porous polymeric matrix for designing an easily separable and recyclable photocatalytic system

Mirabbos Hojamberdiev, Zukhra C. Kadirova, Shahlo S. Daminova, Kunio Yubuta, ... Masashi Hasegawa

Pages 837-846

Purchase PDF Article preview

Research article ○ Abstract only

FEEDBACK

FEEDBACK

FEEDBACK

Research article ○ Abstract only

Selective hydrogenation of 1,3-butadiene over single $Pt_1/Cu(111)$ model catalysts: A DFT study

Cun-Qin Lv, Jian-Hong Liu, Yong Guo, Gui-Chang Wang

Pages 946-955

Purchase PDF Article preview

Research article ○ Abstract only

α-Fe_2O_3 nanoclusters confined into UiO-66 for efficient visible-light photodegradation performance

Rongbin Zhang, Biao Du, Qiuchan Li, Zuqiang Cao, ... Xuewen Wang

Pages 956-963

Purchase PDF Article preview

Previous vol/issue Next vol/issue

ISSN: 0169-4332

Copyright © 2022 Elsevier B.V. All rights reserved

Copyright © 2022 Elsevier B.V. or its licensors or contributors.
ScienceDirect ® is a registered trademark of Elsevier B.V.

ELSEVIER

RELX™

FEEDBACK

ScienceDirect

Applied Surface Science

Supports *open access*

12.1 CiteScore

6.707 Impact Factor

Submit your article

Guide for authors

Menu

Search in this journal

Volume 466

Pages 1-1006 (1 February 2019)

Previous vol/issue

Next vol/issue

Receive an update when the latest issues in this journal are published

Sign in to set up alerts

Full Length Article

Research article ○ Abstract only

DFT study on the influence of sulfur on the hydrophobicity of pyrite surfaces in the process of oxidation

Peng Xi, Changxing Shi, Pingke Yan, Wenli Liu, Ligang Tang

Pages 964-969

Purchase PDF

Article preview

FEEDBACK

Research article ○ Abstract only

Impact of crystal chemistry properties on the collector-mineral interactions observed for REE orthophosphates and oxides

Joanne Gamage McEvoy, Yves Thibault

Pages 970-981

Purchase PDF Article preview

Research article ○ Abstract only

Highly efficient synthesis of 2D VN nanoparticles/carbon sheet nanocomposites and their application as supercapacitor electrodes

Haoyang Wu, Mingli Qin, Zhiqin Cao, Xiaoli Li, ... Xuanhui Qu

Pages 982-988

Purchase PDF Article preview

Research article ○ Abstract only

Low-temperature gas nitriding of AISI 4140 steel accelerated by $LaFeO_3$ perovskite oxide

Xing Chen, Xiangyun Bao, Yang Xiao, Chengsong Zhang, ... Yang Yang

Pages 989-999

Purchase PDF Article preview

Review Article

Review article ○ Abstract only

Review on manganese dioxide for catalytic oxidation of airborne formaldehyde

Lei Miao, Jinlong Wang, Pengyi Zhang

Pages 441-453

Purchase PDF Article preview

VSI: EEPM3 photocatalysis

Research article ○ Abstract only

Carbon-coated Cu-TiO_2 nanocomposite with enhanced photostability and photocatalytic activity

FEEDBACK

Sibo Chen, Xin Li, Wuyi Zhou, Shengsen Zhang, Yueping Fang
Pages 254-261

Purchase PDF Article preview

Research article ○ Abstract only

The effect of N-doped form on visible light photoactivity of Z-scheme g-C_3N_4/TiO_2 photocatalyst

Juan Li, Bowen Li, Qiuye Li, Jianjun Yang
Pages 268-273

Purchase PDF Article preview

Research article ○ Abstract only

Polarization-induced selective growth of Au islands on single-domain ferroelectric $PbTiO_3$ nanoplates with enhanced photocatalytic activity

Chunying Chao, Yisha Zhou, Hao Li, Weiwei He, Wenjun Fa
Pages 274-281

Purchase PDF Article preview

Research article ○ Abstract only

Pt/C@MnO_2 composite hierarchical hollow microspheres for catalytic formaldehyde decomposition at room temperature

Dong Sun, Swelm Wageh, Ahmed A. Al-Ghamdi, Yao Le, ... Chuanjia Jiang
Pages 301-308

Purchase PDF Article preview

Research article ○ Abstract only

$Co_{1.4}Ni_{0.6}P$ cocatalysts modified metallic carbon black/g-C_3N_4 nanosheet Schottky heterojunctions for active and durable photocatalytic H_2 production

Rongchen Shen, Wei Liu, Doudou Ren, Jun Xie, Xin Li
Pages 393-400

Purchase PDF Article preview

Research article ○ Abstract only

Visible-light responsive boron and nitrogen codoped anatase TiO_2 with exposed {001} facet: Calculation and experiment

Rujun Liu, Fan Yang, Yonlong Xie, Ying Yu

FEEDBACK

Pages 568-577

Purchase PDF Article preview

Research article ○ Abstract only

Electroless plating Ni-P cocatalyst decorated g-C_3N_4 with enhanced photocatalytic water splitting for H_2 generation

Kezhen Qi, Yubo Xie, Ruidan Wang, Shu-yuan Liu, Zhen Zhao

Pages 847-853

Purchase PDF Article preview

VSI: Symposium X Spring 2018

Research article ○ Abstract only

Silicon and silicon-germanium nanoparticles obtained by Pulsed Laser Deposition

F. Stock, L. Diebold, F. Antoni, C. Chowde Gowda, ... D. Mathiot

Pages 375-380

Purchase PDF Article preview

VSI: ANGEL2018

Research article ○ Abstract only

Generation of Au nanorods by laser ablation in liquid and their further elongation in external magnetic field

G.A. Shafeev, I.I. Rakov, K.O. Ayyyzhy, G.N. Mikhailova, ... O.V. Uvarov

Pages 477-482

Purchase PDF Article preview

Research article ○ Abstract only

Ablation target cooling by maximizing the nanoparticle productivity in laser synthesis of colloids

Friedrich Waag, Bilal Gökce, Stephan Barcikowski

Pages 647-656

Purchase PDF Article preview

FEEDBACK

Research article ○ Abstract only

Solvent molecules dominated phase transition of amorphous Se colloids probed by in-situ Raman spectroscopy

Qi Chen, Chao Zhang, Jun Liu, Yixing Ye, ... Changhao Liang

Pages 1000-1006

Purchase PDF Article preview

VSI: 15th ISNNM-2018

Research article ○ Abstract only

Iron/carbon composite microfiber catalyst derived from hemoglobin blood protein for lithium-oxygen batteries

Jun-Seo Lee, Hyun-Soo Kim, Won-Hee Ryu

Pages 562-567

Purchase PDF Article preview

Research article ○ Abstract only

Facile phosphorus-embedding into SnS_2 using a high-energy ball mill to improve the surface kinetics of P-SnS_2 anodes for a Li-ion battery

Hongsuk Choi, Seungmin Lee, KwangSup Eom

Pages 578-582

Purchase PDF Article preview

ISSN: 0169-4332

Copyright © 2022 Elsevier B.V. All rights reserved

FEEDBACK

Copyright © 2022 Elsevier B.V. or its licensors or contributors.
ScienceDirect ® is a registered trademark of Elsevier B.V.

FEEDBACK

scimagojr.com/journalsearch.php?q=28983&tip=sid&clean=0

also developed by scimago: SCIMAGO INSTITUTIONS RANKINGS

SJR Scimago Journal & Country Rank

Enter Journal Title, ISSN or Publisher Name

Applied Surface Science

COUNTRY

Netherlands

Universities and research institutions in Netherlands

SUBJECT AREA AND CATEGORY

Chemistry
- Chemistry (miscellaneous)

Materials Science
- Surfaces, Coatings and Films

Physics and Astronomy
- Condensed Matter Physics
- Physics and Astronomy (miscellaneous)
- Surfaces and Interfaces

PUBLISHER

Elsevier

H-INDEX

204

PUBLICATION TYPE

Journals

ISSN

01694332

SCOPE

Applied Surface Science covers topics contributing to a better understanding of surfaces, interfaces, nanostructures and their applications. The journal is concerned with scientific research on the atomic and molecular level of material properties determined with specific surface analytical techniques and/or computational methods, as well as the processing of such structures.

Quartiles

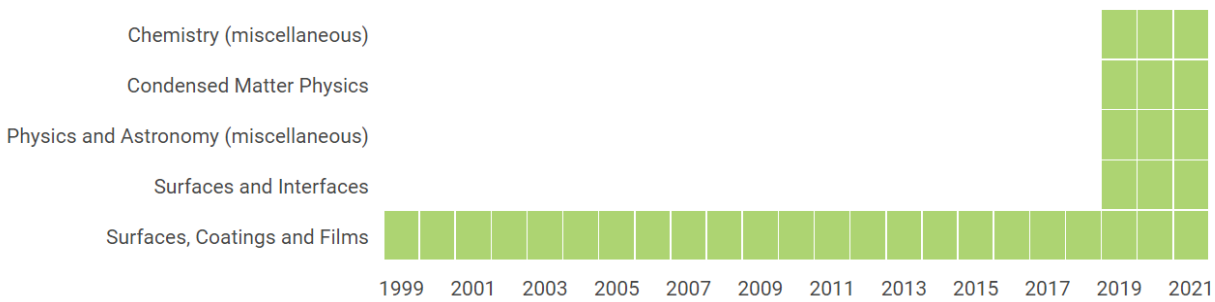

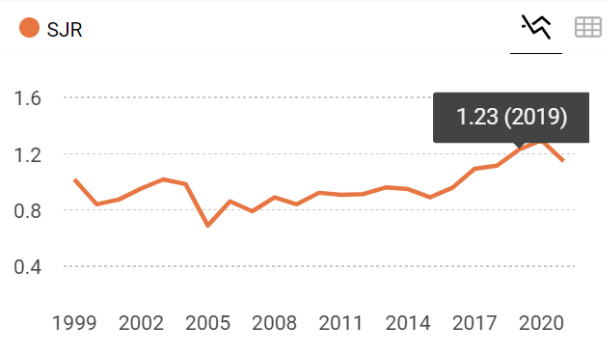

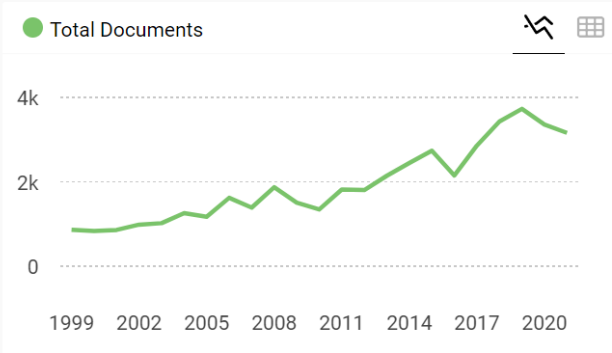

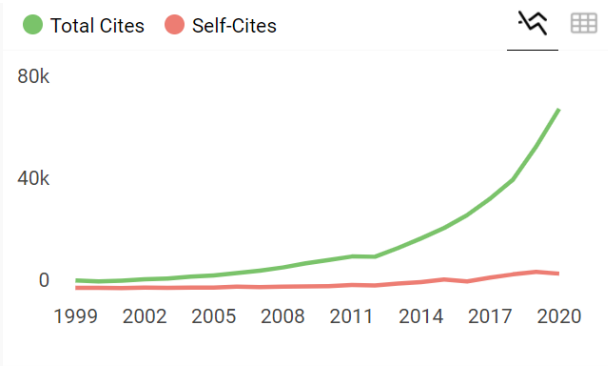

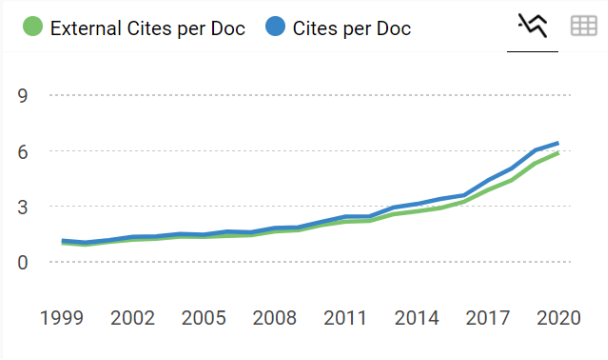

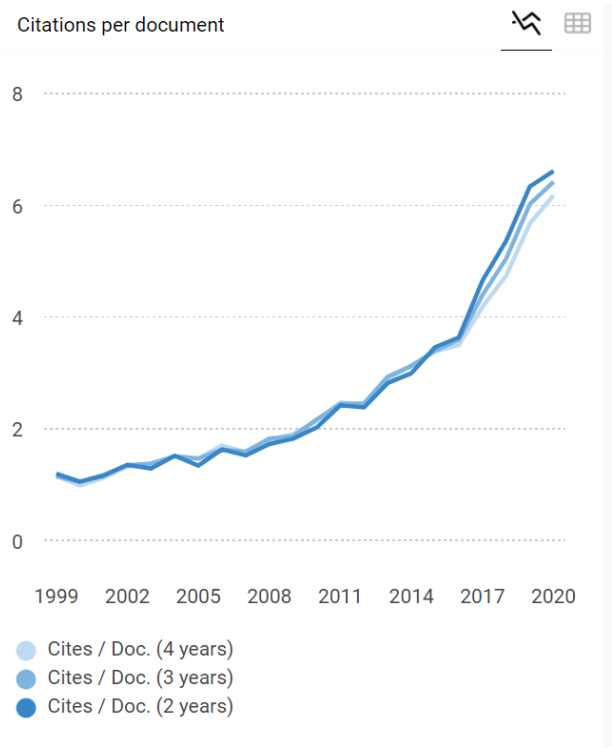

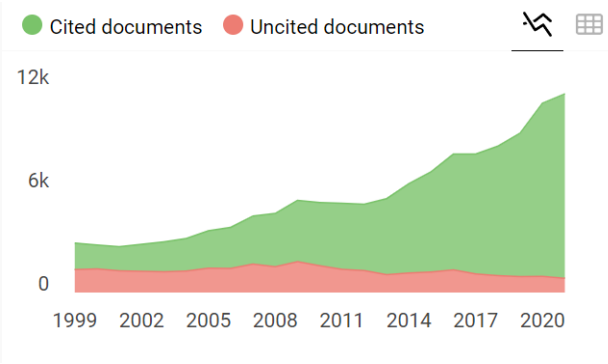

← Show this widget in your own website

Just copy the code below and paste within your html code:

<a href="https://www.scimag

mjl.clarivate.com/search-results

Web of Science Group **Master Journal List** Search Journals Match Manuscript Downloads Help Center Login Create Free Account

NEW The power of the Web of Science™ on your mobile device, wherever inspiration strikes. Dismiss Learn More

APPLIED SURFACE SCIENCE

Publisher:	ELSEVIER , RADARWEG 29, AMSTERDAM, NETHERLANDS, 1043 NX
ISSN / eISSN:	0169-4332 / 1873-5584
Web of Science Core Collection:	Science Citation Index Expanded
Additional *Web of Science* Indexes:	Current Contents Engineering, Computing & Technology | Current Contents Physical, Chemical & Earth Sciences | Essential Science Indicators

Share This Journal View profile page

** Requires free login.*

Applied Surface Science 466 (2019) 352–357

Contents lists available at ScienceDirect

Applied Surface Science

journal homepage: www.elsevier.com/locate/apsusc

Full Length Article

Use of Mn doping to suppress defect sites in Ag_3PO_4: Applications in photocatalysis

Mohammad Afif[a], Uyi Sulaeman[a,*], Anung Riapanitra[a], Roy Andreas[a], Shu Yin[b]

[a] Department of Chemistry, Jenderal Soedirman University, Purwokerto 53123, Indonesia
[b] Institute of Multidisciplinary Research for Advanced Materials, Tohoku University, Sendai 980-8577, Japan

ARTICLE INFO

Keywords:
Ag_3PO_4
Defect sites
Hydroxyl defect
Mn doping
Oxygen vacancy
Photocatalysis

ABSTRACT

The highly active Mn-doped Ag_3PO_4 photocatalyst was successfully synthesized under coprecipitation method using $AgNO_3$, $Na_2HPO_4{\cdot}12H_2O$, and $MnSO_4{\cdot}H_2O$, followed by annealing. The products were characterized using the SEM, XRD, DRS, XPS, and BET. The results showed that the Mn doping decreased the broad absorption in the visible region and increased the atomic ratio of O/Ag. The hydroxyl defects and oxygen vacancies can be suppressed by Mn doping and the photocatalytic activity under visible light irradiation could be improved. This excellent photocatalytic activity was caused by decreasing the recombination of electron and holes due to suppressing the defect sites in the surface of Ag_3PO_4.

1. Introduction

The organic pollutants from the textile industry activities have led to a deterioration of the environment. Therefore, the industries should provide a sewage treatment to handle their pollutants before being sent to the environment. To realize this process, the technology of pollutant destruction using a photocatalyst could be effectively applied for the treatment of organic pollutant. The photocatalyst of TiO_2 has been widely developed to fulfill this goal. However, TiO_2 has a wide band-gap energy that can utilize only ~5% of solar energy. Therefore, another photocatalyst that has high activity under visible light could be expected.

Recently, the silver orthophosphate (Ag_3PO_4), an excellent candidate for the visible light responsive photocatalyst, has been widely studied to be applied for organic pollutant degradation, especially, for the color substances degradation. The methods of composite design [1–3], morphological design [4–7], and doping element [8–11] have been used to prepare the excellent photocatalytic activity.

The high activity of silver orthophosphate photocatalyst has been successfully synthesized using the dopant of cation [8,9], noble metal [11] and mixed anion [12]. Doping Bi^{3+} ions in the crystal can affect the valence band and band gap energy [8]. Under this preparation, Bi^{3+} ions replace P^{5+} ions in Ag_3PO_4 and suppress the hydroxyl (OH) defects on the surface. This design enhances the photocatalytic activity. The Ni^{2+} doping into Ag_3PO_4 can also affect the band gap energy and enhance the separation of electrons and holes pair [9]. The more active species are generated by Ni^{2+} doping because this ion can act as an electron acceptor that lead to the enhanced photocatalytic activity. It is very interesting that the changes of Ag_3PO_4 properties can be controlled by cation doping. The Mn (Mangan) ion, an element with many variations of oxidation number, can be applied for doping in Ag_3PO_4 photocatalyst. However, up to now, Mn ion has not yet been applied for doping in Ag_3PO_4.

Mangan ion has been effectively used as a doping element for photocatalysts. The photocatalysts of TiO_2, $SrTiO_3$, ZnO, SnO_2, and ZnS had been improved by Mn doping [13–17]. The Mn ions doped into the TiO_2 lattice can lead to a redshift of absorption and improves the photocatalytic activity [13]. The Mn^{4+} ion can also be incorporated into $SrTiO_3$ [14]. This ion can substitute the Ti^{4+} ion and shift the absorption toward the visible region. This phenomenon generates the photocatalytic reaction under the visible light irradiation. Incorporation of Mn into ZnO increases the defect site of oxygen vacancy and reduces the band gap energy [15]. This design inhibits the recombination of electrons and holes and improves the photocatalytic properties. A decreased band gap energy and crystal defect can be realized under Mn doping in SnO_2 [16] that increases the photocatalytic activity. Better photocatalytic performances of ZnS can be designed by Mn doping [17] that produces the absorption in the visible region.

Besides doping design, the defects in the lattice of a crystal can influence the photocatalytic activity. These defects can be generated by a doping element and calcination. For examples, the oxygen vacancies

* Corresponding author.
E-mail address: uyi_sulaeman@yahoo.com (U. Sulaeman).

https://doi.org/10.1016/j.apsusc.2018.10.049
Received 7 May 2018; Received in revised form 22 September 2018; Accepted 5 October 2018
Available online 06 October 2018
0169-4332/ © 2018 Elsevier B.V. All rights reserved.

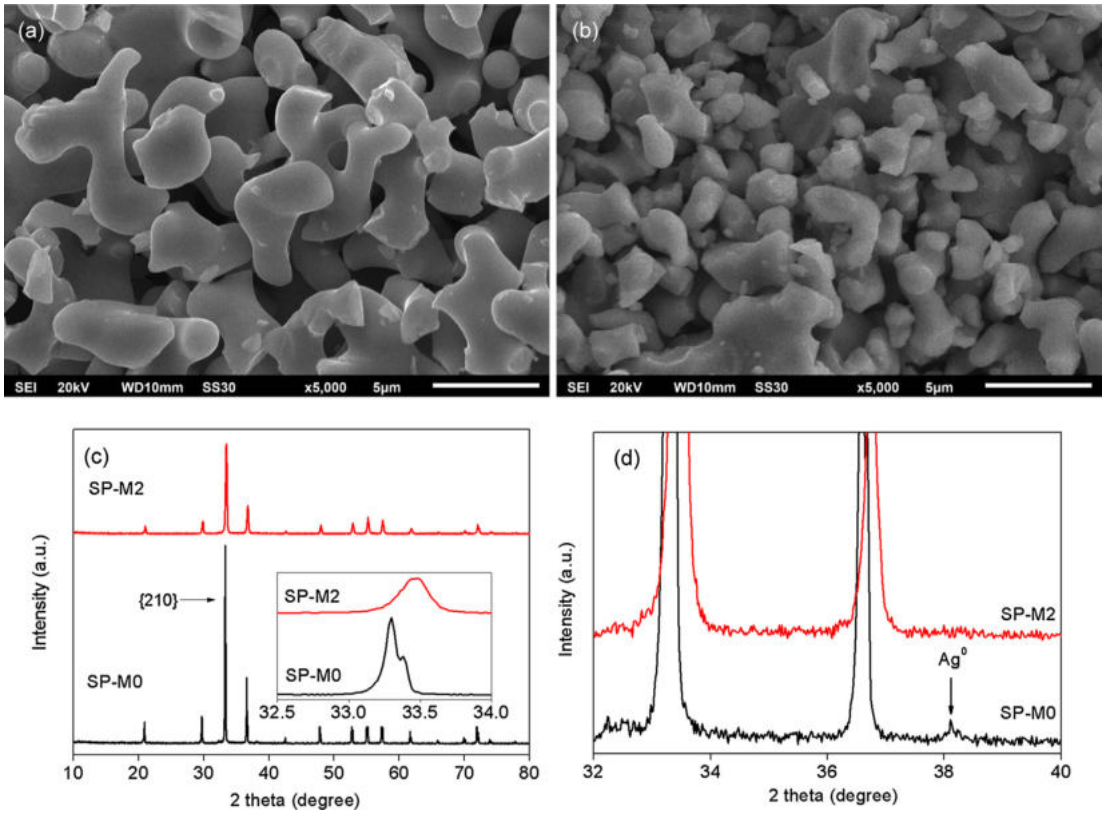

Fig. 1. SEM images of undoped Ag_3PO_4 (SP-M0) (a), Mn-doped Ag_3PO_4 (SP-M2) (b), X-ray diffraction pattern of SP-M0 and SP-M2 (c), and the enlarged XRD pattern of SP-M0 and SP-M2 (d).

in Ag_3PO_4 can be generated by calcination [18]. In a famous photocatalyst, TiO_2, the oxygen vacancies can be formed using a nanotube titanic acid that calcined at various temperatures [19]. In a certain content, the defects can enhance the activity because they increase the separation of electron-hole pairs [20]. However, a much higher defect generated on the lattice leads to being a center of recombination of holes and electrons pair that decreases the photocatalytic activity. Therefore, developing the method for controlling the defect is very useful.

Here, the Mn-doped Ag_3PO_4, for the first time, has been successfully synthesized under coprecipitation method using the starting material of $AgNO_3$, $Na_2HPO_4{\cdot}12H_2O$, and $MnSO_4{\cdot}H_2O$, followed by calcination. The results showed that the Mn doping enhanced the photocatalytic activity by suppressing the hydroxyl defect and oxygen vacancy.

2. Experimental

2.1. Synthesis of samples

The Mn-doped Ag_3PO_4 was synthesized using the coprecipitation method followed by annealing. The starting materials of $MnSO_4{\cdot}H_2O$, $AgNO_3$, $Na_2HPO_4{\cdot}12H_2O$ were used in the experiment. Typically, 1.699 g of $AgNO_3$ was dissolved in 10 ml of water (solution 1) and 1.181 g of $Na_2HPO_4{\cdot}12H_2O$ was dissolved in 20 ml of water (solution 2). The $MnSO_4$ solution (solution 3) was made by adding the $MnSO_4{\cdot}H_2O$ to the 10 ml of water. The amount variation of $MnSO_4{\cdot}H_2O$ was designed at 0.085, 0.169, 0.254, 0.338 and 0.507 g, namely, SP-M1, SP-M2, SP-M3, SP-M4, and SP-M5, respectively. The sample of undoped Ag_3PO_4 (without Mn) was also similarly made, namely SP-M0. The solution 3 was introduced to the solution 1 under magnetic stirring and then the solution 2 was slowly introduced into the mixed solution above until the yellow crystal formed. These products were dried in an oven at 105 °C for 7 h then calcined at 500 °C for 5 h.

2.2. Characterization of samples

The crystal structure was characterized using the XRD (Bruker AXS D2 Phaser). The absorptions of product and band gap energy were investigated using DRS (JASCO V-670). The morphology of the product was determined using SEM (JEOL JSM 7001F) and their specific surface areas were measured using BET (NOVA instruments). The core level of the element and binding energy were investigated using the XPS (Perkin Elmer PHI 5600).

2.3. Photocatalytic evaluation

The photocatalytic activities were investigated under visible light irradiation (LED blue light, Skyled, 3 Watt). Amount of 0.15 g of catalyst was introduced into a 200 ml of 10 mg/L RhB solution. The distance of the sample and the lamp was designed at 10 cm. After keeping the catalyst in the dark solution to achieve the adsorption equilibrium, the photocatalytic reaction was carried out for 15 min. Four ml of sample was withdrawn at the certain interval time and centrifuged at 2000 rpm to separate the catalyst. The concentrations of RhB were measured using the spectrophotometer (Shimadzu 1800).

The reusability of photocatalyst was evaluated. After the photocatalytic reaction, the photocatalysts were recycled, washed and dried at 60 °C for 2 h. These experiments were conducted at 5 cycles.

The mechanisms of photocatalytic reaction were studied using the scavengers to trap the radical and holes under the same condition with the photocatalytic evaluation. The isopropyl alcohol (IPA), ammonium oxalate (AO) and benzoquinone (BQ) with the concentration of 0.1 mmol/L, were used to trap the hydroxyl ($^{\cdot}OH$) radical, holes, and superoxide ion ($O_2^{-\cdot}$) radical, respectively [21,22].

3. Results and discussion

3.1. Characterization

The yellow Ag_3PO_4 crystals were successfully prepared using the co-precipitation of the $AgNO_3$ solution and the Na_2HPO_4 solution followed by calcination. The white solids of Ag_2SO_4 were formed after mixing the $MnSO_4$ and the $AgNO_3$ solution. These white solids disappeared by adding the Na_2HPO_4 solution to the mixed solution and the yellow solids of Ag_3PO_4 were formed. Because the solubility product constant (K_{sp}) of Ag_3PO_4 is lower than that of Ag_2SO_4, the Ag_3PO_4 can easily be precipitated. To investigate the effect of Mn doping, the undoped (SP-M0) and doped (SP-M2) samples were characterized. The bulk grains of 3–5 µm and 2–4 µm were found in SP-M0 and SP-M2 (Fig. 1(a) and (b)) with the specific surface area of 11.3 m^2/g and 17.5 m^2/g, respectively. These morphologies were formed due to the calcination at 500 °C for 7 h. The high temperature might lead to the disordered movement of fine particles leading to the bulk grains [23].

Based on the XRD results (Fig. 1(c)), the Ag_3PO_4 structure exhibits the body-centered cubic (JCPDS No. 06-0505) [2]. There are no impurities such as Ag_2SO_4 found in the samples. The diffraction peak of Mn cannot be observed, indicating that the Mn might be incorporated in a small concentration. The image of {2 1 0} diffraction peak was investigated in detail (see in the inset of Fig. 1(c)). It showed that the shifting of diffraction peak to the higher degree was observed, indicating that the Mn ions might introduce to the crystal lattice of Ag_3PO_4. The doublet of {2 1 0} diffraction peak in SP-M0 suggesting that the large defect sites in SP-M0 might be formed. The small amount of Ag^0 was observed in SP-M0, indicating that the thermal treatment generated the reduction of Ag^+ to Ag^0 (Fig. 1(d)). Incorporating the Mn into the Ag_3PO_4 suppressed the Ag^0 formation since there was no Ag^0 diffraction peak observed in SP-M2.

The absorption in the visible region (above 500 nm) of SP-M0 was larger than that of SP-M2 (Fig. 2), suggesting that the incorporation of Mn into the crystal lattice of Ag_3PO_4 may affect the optical properties of Ag_3PO_4. The large defect formed in the sample of SP-M0 might be generated by the calcination at 500 °C for 5 h. The large absorption in SP-M0 was suppressed by incorporating Mn into the Ag_3PO_4 (SP-M2). It demonstrated that the Mn doping might decrease the large defect of the surface during calcination. To investigate in detail, the band gap energies were calculated using direct optical transition [24] and showing that the 2.28 eV and 2.44 eV were found as the band gap energy of SP-M0 and SP-M2, respectively. The narrowed band gap of SP-M0 might be caused by the high defect crystal which is generated by calcination. Many researchers reported that the calcination generates the defect of oxygen vacancy [18]. After Mn doping, the band gap of Ag_3PO_4 increases to 2.44 eV which agrees with both theoretical (2.43 eV) and experimental value (2.45 eV) [25]. Based on the theory [25], the conduction band of Ag_3PO_4 is mainly attributable to Ag 5s and 5p states, whereas the valence band is dominated by O2p and Ag4d states. It is reasonable that the defect e.g. oxygen vacancy would influence the band gap energy.

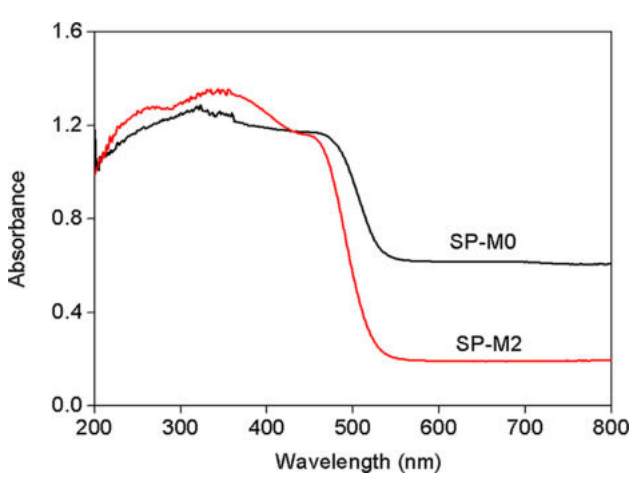

Fig. 2. The absorption spectra of undoped Ag_3PO_4 (SP-M0) and Mn-doped Ag_3PO_4 (SP-M2).

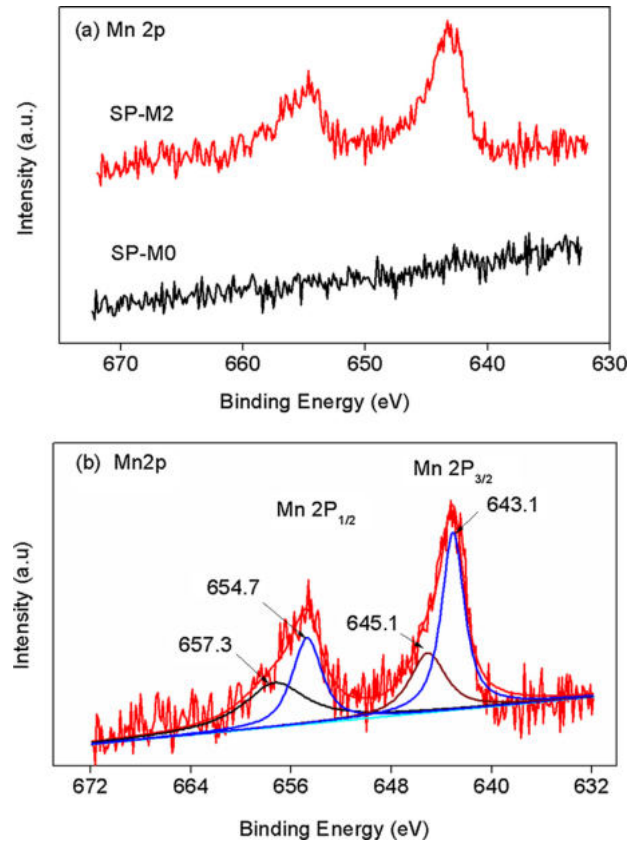

Fig. 3. The XPS of Mn 2p in undoped Ag_3PO_4 (SP-M0) and Mn-doped Ag_3PO_4(SP-M2) (a) and the deconvolution of Mn 2p in SP-M2 (b).

3.2. XPS analysis

To understand the chemical state and composition of Mn-doped Ag_3PO_4, the samples of SP-M0 and SP-M2 were deeply investigated using the XPS. The peak energy of Mn2p was clearly observed, indicating that the Mn was successfully incorporated into Ag_3PO_4 (Fig. 3(a)). The Mn doping in SP-M2 showed the atomic concentration of 2.42% (before sputtering), and 0.67% (after sputtering) as shown in Table 1. The existence of Mn after sputtering, indicating that a portion of Mn introduced to the crystal lattice of Ag_3PO_4. The XPS spectrum of Mn 2p exhibits two peaks at ca. 643.1 and 654.7 eV, which are assigned

Table 1
Surface chemical composition (%) of undoped Ag_3PO_4 (SP-M0) and Mn-doped Ag_3PO_4 (SP-M2) calculated according to XPS analysis.

Samples	Treatment	C1s	O1s	P2p	Mn2p	Ag3d	Ag/P	O/Ag
SP-M0	Before Ar^+ sputtering	16.21	50.25	12.20	0.00	21.34	1.75	2.35
	After Ar^+ sputtering	0.55	45.84	14.74	0.00	39.23	2.66	1.17
SP-M2	Before Ar^+ sputtering	14.65	50.97	11.41	2.42	20.55	1.80	2.48
	After Ar^+ sputtering	0.00	47.45	15.66	0.67	36.21	2.31	1.31

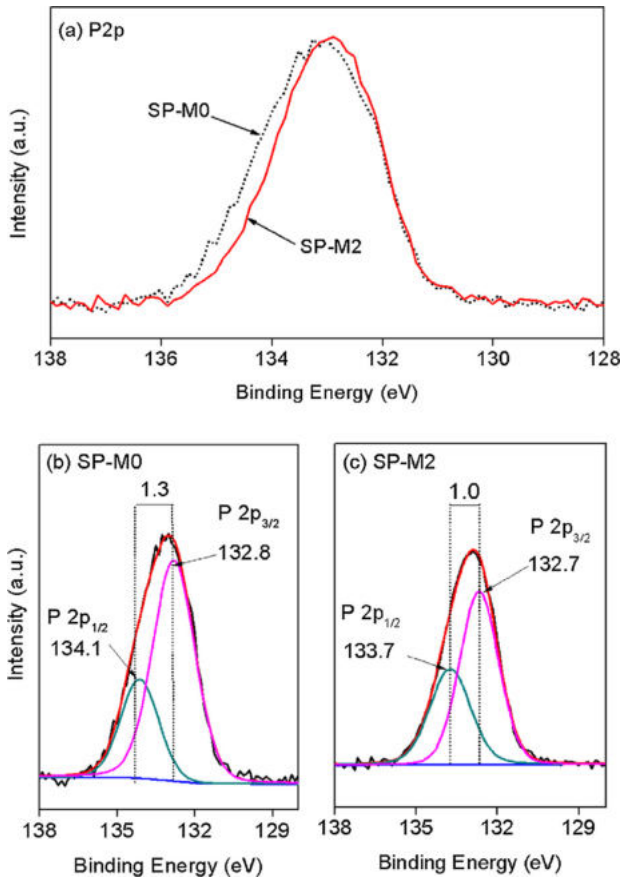

Fig. 4. The XPS of P2p for undoped Ag_3PO_4 (SP-M0) and Mn-doped Ag_3PO_4(SP-M2) (a) and their deconvolution of SP-M0 (b) and SP-M2 (c).

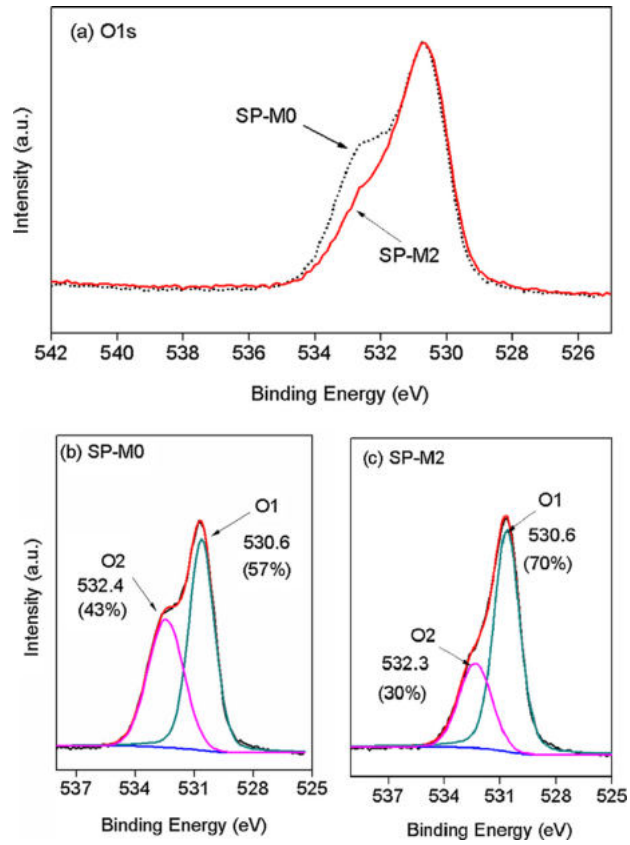

Fig. 5. The XPS of O1s for undoped Ag_3PO_4 (SP-M0) and Mn-doped Ag_3PO_4(SP-M2) (a), and their deconvolution of SP-M0 (b) and SP-M2(c).

to Mn $2p_{2/3}$ and Mn $2p_{1/2}$, respectively, with the spin-orbital splitting of 11.6 eV (Fig. 3(b)). It suggests that the manganese ions are present as Mn^{4+} [26], whereas another peak of 645.1 and 657.3 are assigned to Mn^{5+}. It is possible that the higher oxidation state of Mn could be produced during the annealing. These ions might interstitially be incorporated into Ag_3PO_4 because the ionic radius of Mn^{4+} (39 pm) and Mn^{5+} (33 pm) ions are smaller than those of Ag^+ ions (100 pm) [27]. Moreover, the atomic ratio of Ag/P in Mn-doping is significantly lower than that of the undoped after sputtering (Table 1), indicating that the Mn doping induces the Ag vacancy, therefore the Mn could easily be incorporated in the lattice of the Ag_3PO_4 crystal.

Fig. 4(a) showed that the spectra of P2p in SP-M2 exhibited the shrinkage phenomenon, indicating that the Mn affected the chemical environment of P2p. The deconvolutions of the two spectra are shown in Fig. 4(b) and (c). Two peaks of 134.1 eV and 132.8 eV are assigned to $P2p_{1/2}$ and $P2p_{3/2}$ of SP-M0, respectively, with the spin-orbital splitting of 1.3 eV. Whereas, two peaks of 133.7 eV and 132.7 eV are assigned to $P2p_{1/2}$ and $P2p_{3/2}$ of SP-M2, respectively, with the spin-orbital splitting of 1.0 eV. The Mn incorporation influences the P2p environment that might decrease the spin-orbital splitting.

Fig. 5(a) shows the XPS peak energy of O1s. The deconvolution of SP-M0 and SP-M2 can be seen in Fig. 5(b) and (c), respectively. The O1s spectrum has two peaks of O1 and O2. The lower binding energy of 530.6 eV (O1) is related to O—Ag bonding and the higher binding energy of 532.4 eV is related to OH group [18]. The O2 of SP-M2 exhibits the lower ratio of intensities (30%) compared to that of SP-M0 (43%), indicating that the SP-M2 might have low OH group, whereas the SP-M0 has high OH group in the surface.

The higher intensity ratio of O2 in SP-M0 implying that the undoped Ag_3PO_4 might have large OH defects on the surface. It is similar to those of Bi^{3+} doped Ag_3PO_4 [8], the OH defects are easily created on the surface and replaced the oxygen of P—O tetrahedron due to low energy. Moreover, the high oxygen vacancy might lead to high OH defects. Large OH defects might inhibit the electron excitation and enhance the recombination by breaking the Ag—O bonds. The OH defects also increase the valence band positions and decrease the conduction band, consequently, the band gap becomes narrow. It accords to the band gap calculation from the DRS curve that shows a lower band gap in SP-M0. This phenomenon accelerates the recombination of electron and hole leading to a decreased photocatalytic ability. Because the OH defects generate excess positive charges [8] and doping Mn^{4+} also generate the positive charge, therefore doping Mn^{4+} in Ag_3PO_4 can inhibit the formation of excess OH defects due to the repulsion forces. The OH defects on the surface of Mn-doped Ag_3PO_4 (SP-M2) are significantly lower than that of undoped (SP-M0). Mn^{4+} doping might reduce the OH defects and improve the photocatalytic ability of Ag_3PO_4.

Based on Table 1, the O/Ag atomic ratio of SP-M0 is lower than that of SP-M2 both before and after sputtering, indicating that the oxygen vacancies are really formed in SP-M0. This phenomenon was also supported by the O1s spectrum as shown in Fig. 5. The intensity ratio of O1 in SP-M0 is lower that of SP-M2, suggesting that the O of O—Ag in SP-M0 is in a low concentration. After Mn doping, this detrimental Ag_3PO_4 can be repaired. In addition, the atomic ratio of Ag/P in the SP-M2 (2.31) is significantly lower than that of SP-M0 (2.66) as shown in Table 1 (after sputtering), indicating that the Mn doping also induces the silver vacancy. Therefore, the Mn doping might decrease the defect of hydroxyl radical and oxygen vacancy but increases the silver vacancy. This silver vacancy could also be a crucial role for enhanced catalytic activity. Other researchers [28,29] reported that the thermal treatment generates the silver vacancy in Ag_3PO_4. This phenomenon enhances the separation of photogenerated electrons and holes. The formation of metallic Ag during annealing process could also improve the photocatalytic activity. In our report, however, Mn doping

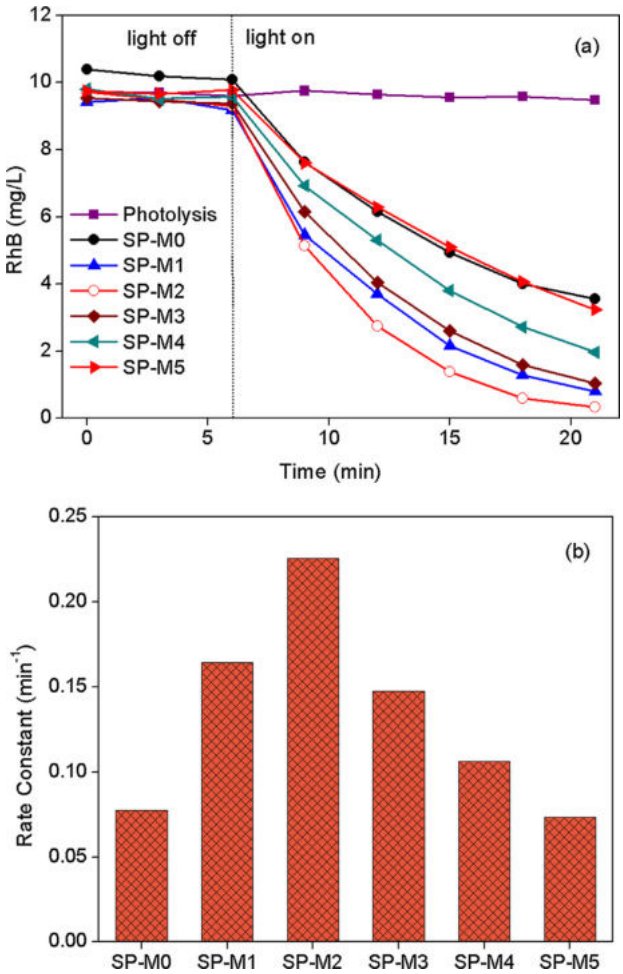

Fig. 6. Photocatalytic activities of Ag_3PO_4 with elevated concentration of doping Mn (a) and their rate constants of pseudo-first-order kinetics (b).

suppresses the formation of metallic Ag.

3.3. Photocatalytic evaluation

Fig. 6 shows the photocatalytic activity of Mn-doped Ag_3PO_4 with the variation of Mn content. The apparent pseudo-first-order kinetics equation of $\ln(C_0/C) = K_{app}t$ was used to study the rate of photocatalytic reaction, where C and C_0 are the RhB concentration at time t and zero, respectively, the K_{app} is the apparent pseudo-first-order rate constant (min^{-1}) [22,30]. The rate of photocatalytic activity has followed the pseudo-first-order kinetics, the rate constant of 0.077 min^{-1}, 0.164 min^{-1}, 0.226 min^{-1}, 0.148 min^{-1}, 0.107 min^{-1} and 0.073 min^{-1} were observed on the samples of SP-M0, SP-M1, SP-M2, SP-M3, SP-M4, and SP-M5, respectively. Incorporating the Mn into the lattice of Ag_3PO_4 affected the photocatalytic activity. The sample of SP-M2 showed the highest activity of ~2.9 times higher compared to that of SP-M0. When the concentration of Mn increases, its photocatalytic activity decreases, indicating that the high concentration of dopant might lead to a negative effect on the catalytic reaction. A too high concentration of dopant might not effectively suppress the defect site of oxygen vacancy.

To evaluate the reusability of Mn-doped Ag_3PO_4, the experiment of RhB photodegradation of SP-M0 and SP-M2 were repeated to 5 cycles (Fig. 7). The results showed that the photocatalytic activity of both SP-M0 and SP-M2 gradually decreased, indicating that the samples were not quite stable. However, the SP-M2 exhibited higher activity compared to that of SP-M0 for all cycles.

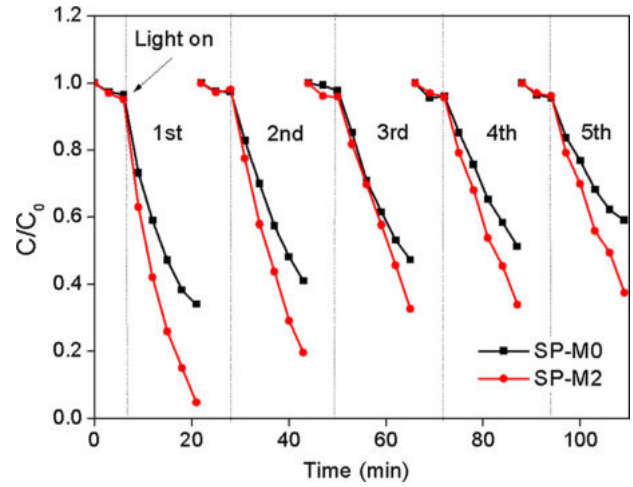

Fig. 7. The recycled photocatalytic reaction of undoped Ag_3PO_4 (SP-M0) and Mn-doped Ag_3PO_4 (SP-M2).

Mechanisms of photocatalytic reaction were studied by adding the scavengers of radicals and holes [21,22]. The IPA, AO, and BQ were added to the reaction solution as the scavenger of $^{\cdot}OH$, h^+ and $O_2^{-\cdot}$, respectively. The effect of these scavengers to the photocatalytic reaction can be seen in Fig. 8. The mechanisms of SP-M0 and SP-M2 are similar, both SP-M0 and SP-M2 are greatly suppressed by the AO and BQ, as shown in Fig. 8(a), indicating that the mechanism involve mostly

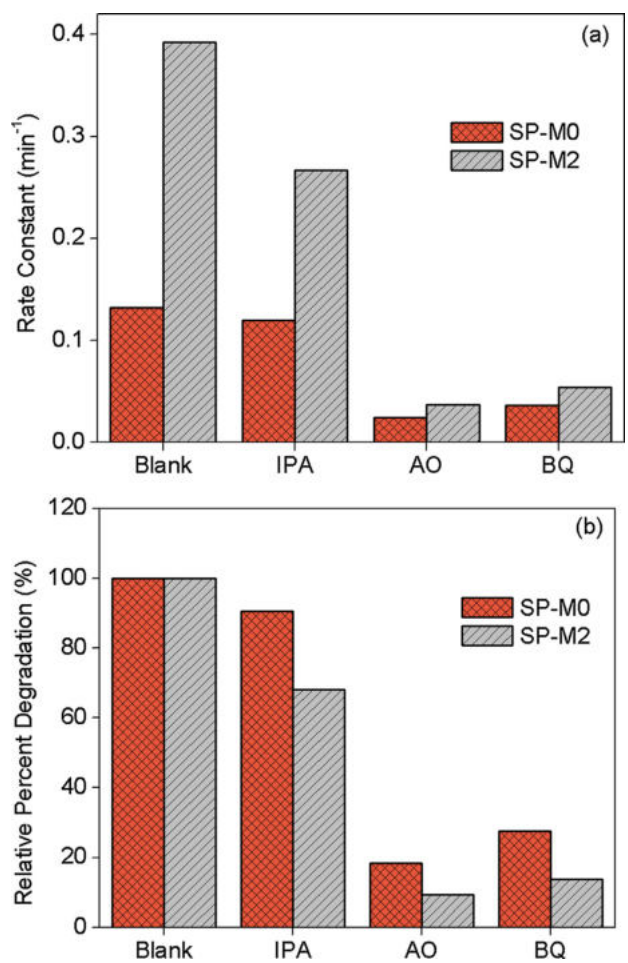

Fig. 8. The effect of scavengers on the rate constant of photocatalytic activity (a) and their relative percent degradations (b).

via h^+ and $O_2^{-\cdot}$. To understand the rate mechanism in SP-M0 and SP-M2, the rate constants of photocatalytic activity were compared to the blank one (relative percent degradation) as shown in Fig. 8(b). The results showed that relative percent degradations in SP-M2 due to scavenger of IPA, AO and BQ are lower than that of SP-M0, indicating that the role of $^{\cdot}OH$, h^+, and $O_2^{-\cdot}$ scavenger works more efficiently in SP-M2. It is because the effect of Mn doping effectively inhibits the recombination of electron and hole pairs due to suppressing the defect sites in the surface.

4. Conclusions

The Mn could be easily incorporated into the crystal lattice of Ag_3PO_4 using the coprecipitation method followed by calcination. The Mn doping decreased the broad absorption in the visible region and increased the atomic ratio of O/Ag. Large OH defect and oxygen vacancy might be generated in the sample without Mn doping during calcination. These large defects could effectively be suppressed by doping with Mn and improved the photocatalytic activity.

Acknowledgments

This research was supported by the Ministry of Research, Technology and Higher Education of the Republic of Indonesia in the Scheme of Competency Grant, Contract Number: 059/SP2H/LT/DRPM/2018. It was also partly supported by the JSPS KAKENHI Grant Number JP16H06439 (Grant-in-Aid for Scientific Research on Innovative Areas), the Dynamic Alliance for Open Innovation Bridging Human, Environment and Materials, the Cooperative Research Program of “Network Joint Research Center for Materials and Devices”.

References

[1] T. Zhou, G. Zhang, P. Ma, X. Qiu, H. Zhang, H. Yang, G. Liu, J. Alloys Compd. 735 (2018) 1277–1290.
[2] X. Cui, L. Tian, X. Xian, H. Tang, X. Yang, Appl. Surf. Sci. 430 (2018) 108–115.
[3] H. Wang, L. Zou, Y. Shan, X. Wang, Mater. Res. Bull. 97 (2018) 189–194.
[4] U. Sulaeman, F. Febiyanto, S. Yin, T. Sato, Catal. Commun. 85 (2016) 22–25.
[5] L. Wang, L. Wang, D. Chu, Z. Wang, Y. Zhang, J. Sun, Catal. Commun. 88 (2017) 53–55.
[6] C. Zheng, H. Yang, Y. Yang, J. Ceram. Soc. Jpn. 125 (2017) 141–144.
[7] R. Guo, Y. Fan, Y. Tang, RSC Adv. 7 (2017) 23977–23981.
[8] S. Zhang, S. Zhang, L. Song, Appl. Catal. B 152–153 (2014) 129–139.
[9] L. Song, Z. Chen, T. Li, S. Zhang, Mater. Chem. Phys. 186 (2017) 271–279.
[10] M.S.A. Hussien, I.S. Yahia, J. Photochem. Photobiol. A 356 (2018) 587–594.
[11] T. Yan, H. Zhang, Y. Liu, W. Guan, J. Long, W. Li, J. You, RSC Adv. 4 (2014) 37220–37230.
[12] W. Cao, Z. Gui, L. Chen, X. Zhu, Z. Qi, Appl. Catal. B 200 (2017) 681–689.
[13] Q.R. Deng, X.H. Xia, M.L. Guo, Y. Gao, G. Shao, Mater. Lett. 65 (2011) 2051–2054.
[14] G. Wu, P. Li, D. Xu, B. Luo, Y. Hong, W. Shi, C. Liu, Appl. Surf. Sci. 333 (2015) 39–47.
[15] N.A. Putri, V. Fauzia, S. Iwan, L. Roza, A.A. Umar, S. Budi, Appl. Surf. Sci. 439 (2018) 285–297.
[16] B. Babu, A.N. Kadam, G.T. Rao, S.W. Lee, C. Byond, J. Shim, J. Lumin. 195 (2018) 283–289.
[17] L. Wang, P. Wang, B. Huang, X. Ma, G. Wang, Y. Dai, X. Zhang, X. Qin, Appl. Surf. Sci. 391 (2017) 557–564.
[18] R. Chong, X. Cheng, B. Wang, D. Li, Z. Chang, L. Zhang, Int. J. Hydrogen Energy 41 (2016) 2575–2582.
[19] L. Hou, M. Zhang, Z. Guan, Q. Li, J. Yang, Appl. Surf. Sci. 428 (2018) 640–647.
[20] J. Yan, G. Wu, N. Guan, L. Li, Z. Li, X. Cao, Phys. Chem. Chem. Phys. 15 (2013) 10978–10988.
[21] W. Liu, M. Wang, C. Xu, S. Chen, X. Fu, Mater. Res. Bull. 48 (2013) 106–113.
[22] U. Sulaeman, D. Hermawan, R. Andreas, A.Z. Abdullah, S. Yin, Appl. Surf. Sci. 428 (2018) 1029–1035.
[23] V. Stengl, S. Bakardjieva, N. Murafa, V. Houskova, K. Lang, Microporous Mesoporous Mater. 110 (2008) 2575–2582.
[24] M.A. Butler, J. Appl. Phys. 48 (1977) 1914–1920.
[25] J.J. Liu, X.L. Fu, S.F. Chen, Y.F. Zhu, Appl. Phys. Lett. 99 (2011) 191903.
[26] Q. Li, G. Li, C. Fu, D. Luo, J. Fan, D. Xie, L. Li, J. Mater. Chem. A 3 (2015) 10592–10602.
[27] R.D. Shannon, Acta Cryst. A32 (1976) 751–767.
[28] T. Yan, W. Guan, J. Tian, P. Wang, W. Li, J. You, B. Huang, J Alloys Compd. 680 (2016) 436–445.
[29] T. Yan, W. Guan, Y. Xiao, J. Tian, Z. Qiao, H. Zhai, W. Li, J. You, Appl. Surf. Sci. 391 (2017) 592–600.
[30] Y. Li, X. Li, J. Li, J. Yin, Water Res. 40 (2006) 1119–1126.